

# Structure and mechanism of the epoxide hydrolase from *Agrobacterium radiobacter* AD1

Marco Nardini<sup>a</sup>, Rick Rink<sup>b</sup>, Dick B. Janssen<sup>b</sup>, Bauke W. Dijkstra<sup>a,\*</sup>

<sup>a</sup> *Laboratory of Biophysical Chemistry and BIOSON Research Institute, University of Groningen, Nijenborgh 4, Groningen 9747 AG, Netherlands*

<sup>b</sup> *Laboratory of Biochemistry, Department of Chemistry, University of Groningen, Nijenborgh 4, Groningen 9747 AG, Netherlands*

## Abstract

The X-ray structure of the epoxide hydrolase from *Agrobacterium radiobacter* AD1 has been determined by isomorphous replacement at 2.1 Å resolution. The enzyme shows a two-domain structure, with the core having the  $\alpha/\beta$  hydrolase fold topology which provides the scaffolding for the catalytic triad residues, Asp 107, Asp 246, and His 275. Based on biochemical and structural data, a mechanism is proposed to illuminate the peculiar chemical strategy to activate harmful epoxide substrates for hydrolysis and detoxification. The structure suggests Tyr 152/Tyr 215 as the residues involved in substrate binding, stabilization of the transition state, and possibly protonation of the epoxide oxygen. Site-directed mutagenesis studies confirmed the structural results and, in addition, showed a significant increase in enantioselectivity for styrene oxide, and substituted variants thereof, for a Tyr 215  $\rightarrow$  Phe mutant. Since Tyr 215 is conserved among all epoxide hydrolase sequences, an activating role of this residue is suggested for other epoxide hydrolases as well, and mutation of this residue might also result in mutant enzymes with improved enantioselectivity in other cases. © 2001 Elsevier Science B.V. All rights reserved.

**Keywords:** Crystal structure; Epoxide hydrolase;  $\alpha/\beta$  hydrolase fold; Nucleophile

## 1. Introduction

Epoxide hydrolases (EC 3.3.2.3) comprise a group of enzymes that catalyze the two-step hydrolytic cleavage of reactive and toxic epoxides to yield the corresponding diols [1]. The first half-reaction involves the formation of a covalent ester intermediate at the carboxylate of the nucleophile. In the second

half-reaction, the ester intermediate is hydrolyzed by a water molecule activated by a His/Asp pair [2–4].

Epoxide hydrolases are ubiquitous in nature, having been found in various species of plants, insects, bacteria, and mammals. They can be grouped into soluble and microsomal epoxide hydrolases on the basis of their cellular localization and biochemical properties [1]. The major biochemical role of these enzymes is the degradation of epoxide compounds. Epoxides are frequently found as intermediates in the catabolic pathway of several xenobiotics and, being electrophilic in nature, they can easily react with various biological nucleophiles. The degradation of

\* Corresponding author. Tel.: +31-50-363-4381; fax: +31-50-363-4800.

E-mail address: bauke@chem.rug.nl (B.W. Dijkstra).

such potentially harmful compounds to more polar metabolites is therefore of great importance for living cells.

Because of their central role in detoxification processes of drugs and toxic compounds, mammalian epoxide hydrolases have been studied for many years [2,3,5–9]. However, recently important results have been achieved in the expression and characterization of bacterial epoxide hydrolases as well, opening a new exciting field of research [4,10–12]. Bacterial epoxide hydrolases can easily be produced in large amount and, since they exhibit enantioselectivity for many industrially important epoxides, they have a great biotechnological potential in the large-scale preparation of optically active epoxides and diols by kinetic resolution [1,13].

So far, the characterization and the insights into the catalytic mechanism of this class of enzymes have been based mainly on biochemical studies. Information on their three-dimensional structures was indirectly derived on the basis of the low, but significant, sequence similarity with haloalkane dehalogenase from *Xanthobacter autotrophicus* GJ10 of which the structure is known [4,5]. Very recently, we reported the structure determination of the epoxide hydrolase from *Agrobacterium radiobacter* AD1 [14]. The availability of this first epoxide hydrolase structure allows us to answer in atomic details important open questions about catalysis by these enzymes.

## 2. Materials and methods

### 2.1. Crystallization

The epoxide hydrolase from *A. radiobacter* AD1 (Ephy) was cloned, overexpressed, and purified as described previously [4]. Ephy was crystallized by the hanging drop method. Drops containing 4  $\mu$ l of protein solution and 4  $\mu$ l of precipitant were equilibrated against a 1 ml reservoir containing 1.6–1.8 M  $\text{KH}_2\text{PO}_4/\text{K}_2\text{HPO}_4$  (pH 7.0) at room temperature. After 2 weeks, the experiments were allowed to slowly evaporate to a phosphate concentration of about 2.0 M. The slow increase of the phosphate concentration in the drop results in the appearance of

crystals with typical sizes of  $0.3 \times 0.2 \times 0.1 \text{ mm}^3$ . They are highly X-ray-sensitive and therefore, all data collections were performed at cryotemperature (100 K), using 30% glycerol added to the stabilizing mother liquor (1.8 M  $\text{KH}_2\text{PO}_4/\text{K}_2\text{HPO}_4$ ) as a cryoprotectant.

The crystals diffract up to 2.1  $\text{\AA}$  resolution using synchrotron radiation and belong to space group C2 with unit cell parameters of  $a = 146.62 \text{ \AA}$ ,  $b = 100.20 \text{ \AA}$ ,  $c = 96.88 \text{ \AA}$ ,  $\beta = 100.68^\circ$ . This unit cell gives a  $V_M$  value of  $2.57 \text{ \AA}^3 \text{ Da}^{-1}$ , assuming four molecules in the asymmetric unit.

### 2.2. Structure determination and quality of the model

The Ephy X-ray structure has been determined by the isomorphous replacement method supplemented by anomalous scattering (SIRAS), using ethyl mercury phosphate,  $(\text{C}_2\text{H}_5\text{HgO})_3\text{PO}$ , as the single heavy atom derivative [14]. Data sets were collected in-house and at the X-ray diffraction beamline of the ELETTRA synchrotron in Trieste (Italy). The final model consists of  $4 \times 282$  residues, 610 water molecules (33 of them refined with double positions) and four potassium ions, originating from the crystallization buffer (one for each molecule in the asymmetric unit). In each monomer (294 residues), the first N-terminal residue (Met) is not visible, nor is there interpretable electron density map for the loop 138–148. The final crystallographic  $R_{\text{factor}}$  and  $R_{\text{free}}$  values are 19.0% and 22.7%, respectively. The rms deviations from ideal geometry are 0.008  $\text{\AA}$  for bond lengths and  $1.338^\circ$  for bond angles. No residues are in the disallowed regions of the Ramachandran plot. Pro 39 was found in a *cis*-peptide conformation. The atomic coordinates and the structure factors have been deposited with the Protein Data Bank (entry code 1ehy).

## 3. Results and discussion

### 3.1. Global fold

The Ephy monomer has a nearly globular shape and consists of two domains: a ‘core’ domain, which shows the typical features of the  $\alpha/\beta$  hydrolase fold

topology [15], and a mainly  $\alpha$ -helical second domain, which lies like a ‘cap’ on top of the core domain (Fig. 1).

The core domain consists of a central eight-stranded  $\beta$ -sheet with seven parallel strands (only the second strand is antiparallel). Its topology is  $+1, +2, -1x, +2x, (+1x)_3$  and it displays a left-handed superhelical twist with the first and the last strands crossing each other at an angle greater than  $90^\circ$ . The  $\beta$ -sheet is flanked on both sides by  $\alpha$ -helices, two on one side and four on the other. Helices  $\alpha 1, \alpha 2, \alpha 3, \alpha 9, \alpha 10$  and  $\alpha 11$  correspond to helices  $\alpha A, \alpha B, \alpha C, \alpha D, \alpha E$  and  $\alpha F$  of the ‘canonical’  $\alpha/\beta$  hydrolase fold [16]. Compared to the ‘canonical’ fold, an extra  $3_{10}$  helix is present at the N-terminus of Ephy. Short  $3_{10}$  helices are also located one residue before helices  $\alpha 1$  and  $\alpha 2$ , and one residue after helix  $\alpha 3$ , but they can be considered as extensions of the ‘canonical’  $\alpha$ -helices.  $\alpha 9$  is a one-turn  $3_{10}$  helix, and  $\alpha 11$  is divided in two parts due to the presence of a proline residue in the center of the helix (Fig. 2).

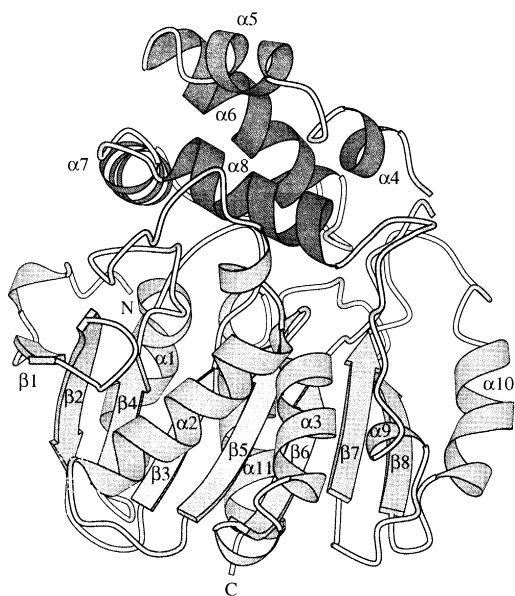


Fig. 1. Schematic view of the secondary structure elements of epoxide hydrolase. Ribbon representation drawn using MOLSCRIPT [22];  $\alpha$ -helices,  $\beta$ -strands and coils are represented by helical ribbons, arrows and ropes, respectively. The  $\alpha$ -helices of the cap domain are shown in dark gray.

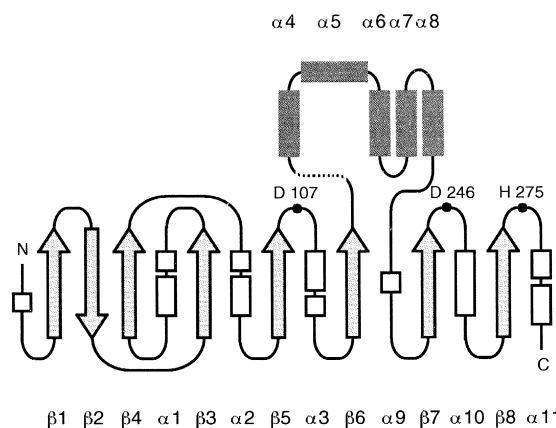


Fig. 2. Secondary structure topology diagram, and location of the catalytic triad residues, Asp 107, Asp 246, and His 275. The dashed line represents the missing loop 138–148.  $\alpha$ -helices and  $\beta$ -strands are represented by rectangles and arrows, respectively.  $3_{10}$  helices are shown by squares. The  $\alpha$ -helices of the cap domain are shown in dark gray.

The cap domain, containing helices  $\alpha 4$ – $\alpha 8$ , forms a large excursion between  $\beta$ -strands  $\beta 6$  and  $\beta 7$  of the  $\alpha/\beta$  hydrolase domain (Fig. 2). It has a double-layered structure with helices  $\alpha 7$  and  $\alpha 8$  located between the core domain and the plane formed by  $\alpha 4, \alpha 5$  and  $\alpha 6$  (Fig. 1).

### 3.2. Active site

The active site cavity is located in a predominantly hydrophobic environment, between the core and the cap domain. The core domain provides the scaffolding for the catalytic triad residues Asp 107, His 275, and Asp 246, whereas the  $\alpha$ -helical cap domain contributes several residues important for the interaction with substrates.

Asp 107 is situated at the very sharp ‘nucleophile elbow’ between the central strand  $\beta 5$  and helix  $\alpha 3$ , where it can be easily approached by the substrate as well as by the hydrolytic water molecule. In Ephy, the ‘nucleophile elbow’ is identified by the consensus sequence Gly–His–Asp–Phe–Ala, corresponding to the ‘canonical’ Sm–X–Nu–X–Sm (Sm = small residue, X = any residue, Nu = nucleophile). The tightness of this strand-turn-helix motif causes the nucleophile Asp 107 to adopt energetically unfav-

avorable main chain torsion angles ( $\phi = 57^\circ$ ,  $\psi = -124^\circ$ ) and imposes steric restrictions on the residues located in its proximity. The nucleophile conformation is stabilized by a network of hydrogen bonds involving residues of the sharp turn, as has been found in other  $\alpha/\beta$  hydrolase enzymes. In addition, the main chain nitrogen atom of Asp 107 interacts via a hydrogen bond with the backbone oxygen atom of Asp 131. Furthermore, the side chain of Asp 107 is stabilized by a hydrogen bond of its O $\delta$ 2 atom with the backbone amide groups of Trp 38 and Phe 108, and by a salt bridge between its O $\delta$ 1 atom and the N $\epsilon$ 2 atom of the His 275 side chain (Fig. 3).

The catalytic His 275 is located in a loop between strand  $\beta$ 8 and helix  $\alpha$ 11, in a position absolutely conserved within the  $\alpha/\beta$  hydrolase fold enzymes [15,16].

The acidic member of the catalytic triad, Asp 246, assists His 275 in activating the water molecule which hydrolyzes the ester intermediate formed at Asp 107 [4]. Asp 246 is located in a turn between strand  $\beta$ 7 and helix  $\alpha$ 10, in a position topologically conserved within the  $\alpha/\beta$  hydrolase fold family [15,16]. However, in the Ephy crystal structure, Asp 246 is not at interacting distance from His 275. Instead, the loop containing this residue is pulled away from the active site and the Asp 246 side chain is pointing into the solvent. This is probably the result of crystal packing forces since helix  $\alpha$ 10, which follows the loop containing Asp 246 (Fig. 2), is involved in an intermolecular contact with the

same helix from another molecule in the asymmetric unit (interaction between molecules A/B, and C/D).

The space vacated by Asp 246 makes it possible for the side chain of Gln 134 to move into the active site, occupying the site where the substrate is likely to be bound (Fig. 3). Its position is stabilized by a hydrogen bonding network involving the hydroxyl groups of Tyr 152 and Tyr 215, and the carboxyl oxygen O $\delta$ 1 of Asp 107. Tyr 152, Tyr 215, together with Trp 183, are supplied by the cap domain, which is responsible for sealing and shaping the upper part of the active site cavity. Remodeling of the structure to its supposed active conformation positions Asp 246 at direct interacting distance to the catalytic His 275, and puts Gln 134 close to the surface of the enzyme [14]. This result is confirmed by a Gln 134  $\rightarrow$  Ala mutation, which is only little affected in its steady-state kinetics compared to wild-type enzyme, indicating that Gln 134 is not essential for catalysis [17]. Moreover, the *A. radiobacter* epoxide hydrolase shows competitive inhibition by amides, especially by compounds like phenylacetamide ( $K_i = 30 \mu\text{M}$ ) [17]. Therefore, we conclude that in the crystal structure, the Gln 134 side chain may act as such as an inhibitor, mimicking the binding mode of epoxide substrates. Docking (with the program GRID [18]) of phenylacetamide in the active site cavity of the remodeled *A. radiobacter* epoxide hydrolase indeed positions its amide moiety in a region between the hydroxyl groups of Tyr 152 and Tyr 215, and the carboxyl oxygen O $\delta$ 1 of Asp 107, and the

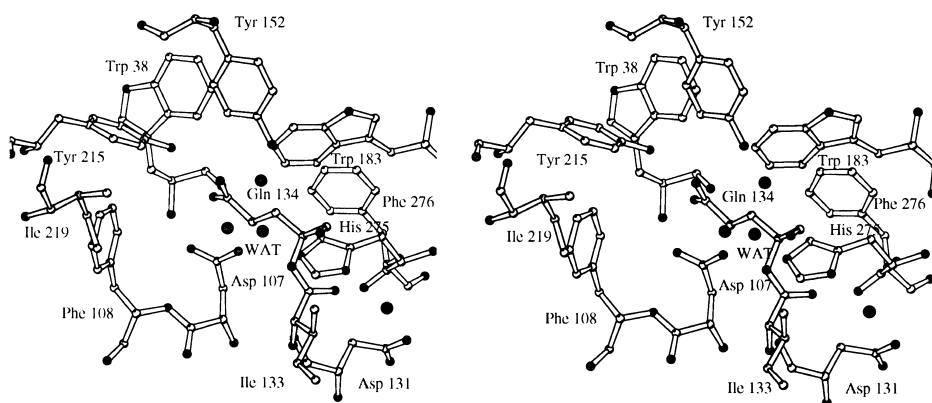


Fig. 3. Stereo view of residues lining the active site of epoxide hydrolase. Residues and water molecules are drawn in ball-and-stick representation using MOLSCRIPT [22]. The catalytic water molecule is labelled "WAT".

aromatic tail of the inhibitor in a highly hydrophobic pocket lined by Phe 108, Ile 133, Phe 137, Ser 153, and Ile 219 side chains (Fig. 4). The docking of the phenylacetamide inhibitor provides a plausible picture of the binding mode of substrate such as styrene oxide, and substituted variants thereof.

### 3.3. Reaction mechanism

On the basis of biochemical data and site-specific mutations, a two-step catalytic mechanism was proposed for Ephy [4]. In the first reaction step, an ester bond is formed between enzyme and substrate by attack of the nucleophilic Asp 107 on the primary carbon of the substrate; in the second step, this ester bond is hydrolyzed by a water molecule activated by the His 275/Asp 246 pair. The reaction proceeds via two different transition states, one during the binding and opening of the epoxide ring, the second during the hydrolysis of the ester intermediate.

The X-ray structure localizes the catalytic Asp 107 and His 275 in a hydrophobic cavity located between the core and the cap domains. Furthermore, the active site cavity contains two tyrosine residues: Tyr 152 and Tyr 215 (Fig. 3). These two tyrosines are the only acidic functional groups present in the active site that can facilitate the opening of the epoxide ring by hydrogen bonding and protonating the epoxide oxygen during the first step of catalysis. In agreement with this hypothesis, mutagenesis studies of these tyrosines have shown that only a double

Tyr → Phe mutant is completely inactive, suggesting that both Tyr 152 and Tyr 215 are able to provide the proton needed for the opening of the epoxide ring [17,19]. Since Tyr 215 is absolutely conserved within the epoxide hydrolase family and Tyr 152 is mostly conserved in the soluble epoxide hydrolases, it is likely that the Tyr activation is a general property of this class of enzymes (Fig. 5). In the *A. radiobacter* epoxide hydrolase, the resulting tyrosinate could be stabilized by a hydrogen bonding interaction with the other tyrosine, and by edge-to-face interactions with the neighboring aromatic residues Phe 108 and His 156. A similar stabilizing interaction has been also proposed for a recently solved epoxide hydrolase from mouse [20]. Reprotonation of the tyrosinate could occur from the bulk solvent, although a precise pathway is difficult to assign.

The X-ray structure provides also important information about the hydrolysis step. Indeed, a water molecule is visible at hydrogen bond distance from the N $\epsilon$ 2 atom of the His 275 side chain. Due to the crystallization pH (7.0) in the X-ray structure, His 275 is stabilized by a salt bridge with Asp 107 O $\delta$ 1. At the optimum pH for catalysis (8.4–9.0), His 275 N $\epsilon$ 2 is most likely deprotonated and therefore able to activate the water molecule located nearby. In the crystal structure, this water molecule is in contact with the solvent via a narrow tunnel located between  $\alpha$ -helices  $\alpha$ 1,  $\alpha$ 10, the loop connecting helix  $\alpha$ 1 and strand  $\beta$ 3 of the core domain, and  $\alpha$ 7 of the cap

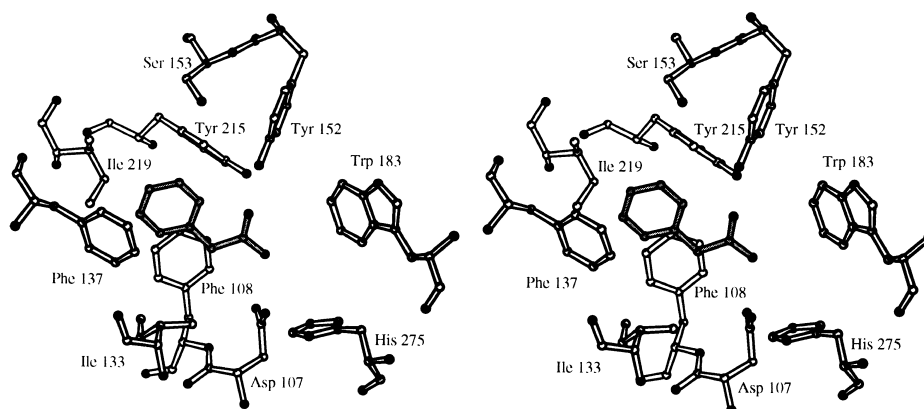


Fig. 4. Stereo view of the phenylacetamide inhibitor (grey color) docked in the active site cavity of the remodeled epoxide hydrolase structure. Residues and inhibitor molecule are drawn in ball-and-stick representation using MOLSCRIPT [22].

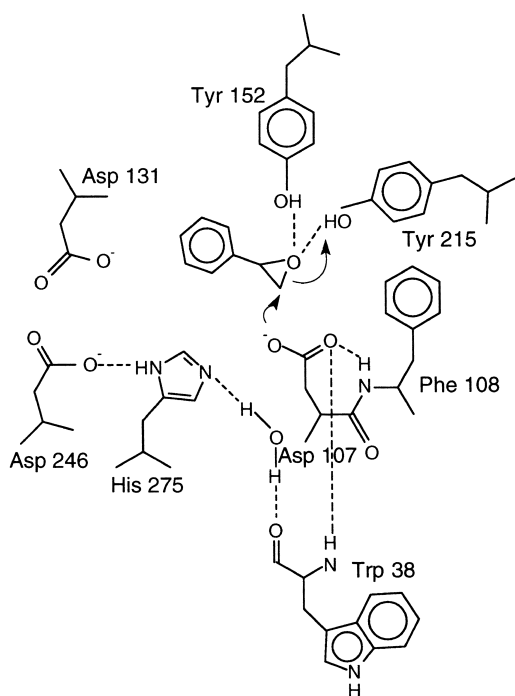


Fig. 5. Schematic representation of the catalytic mechanism of epoxide hydrolase. The Michaelis complex with styrene oxide is shown just before the formation of covalent intermediate, which is indicated by arrows. Hydrogen bonds are shown as dashed lines.

domain. This tunnel leads to the back of the active site cavity, and it is perfectly suited to replenish the hydrolytic water molecule at hydrogen bond distance from the His 275 N $\delta$ 2 atom after the reaction. In our structure, the active site cavity is exposed to the solvent from the front part, too, where the missing loop 138–148 is located. Due to the position of the hydrolytic water molecule in the back of the active site, it is likely that the substrate enters the active site cavity from the front part.

During the hydrolysis of the ester intermediate, the negative charge that develops on the nucleophile side chain must be stabilized. In epoxide hydrolases, as in many other members of the  $\alpha/\beta$  hydrolase fold family, the peculiar geometry of the 'nucleophile elbow' contributes to the formation of part of the oxyanion binding site, which stabilizes the negatively charged transition state occurring during hydrolysis [15]. This 'oxyanion hole' is formed by two backbone nitrogen atoms: the first is from Phe 108, which is the residue immediately following the nu-

cleophile, whereas the second is from Trp 38 (Fig. 3). The latter residue is located between strand  $\beta$ 3 and helix  $\alpha$ 1, and it is part of a HGxP tetrapeptide motif (x = any amino acid) conserved in epoxide hydrolases and other  $\alpha/\beta$  hydrolase fold enzymes [4,14]. The HGWP motif of Ephy is located in a sharp *cis*-proline turn (Trp 38–Pro 39), which is stabilized by the hydrogen bond between His 36 N $\delta$ 1 and the backbone carbonyl oxygen of Gly 37.

### 3.4. Structure and site-directed mutagenesis relationship

In the recent past, a site-directed mutagenesis approach was used on Ephy to further analyse residues potentially important for catalysis. This confirmed the residues of the catalytic triad, Asp 107, His 275, and Asp 246 [4]. However, although the latter residue was found to be important for catalysis, it was not absolutely essential, since an Asp 246  $\rightarrow$  Ala mutant still displayed some residual activity ( $\sim$ 0.5% of the wild-type activity) [4]. The three-dimensional structure of Ephy gives clear clues to explain the behaviour of this mutant. The structure shows that another aspartic acid, Asp 131, is present, which may act as a backup of Asp 246. Asp 131 is located between strand  $\beta$ 6 and the first helix of the cap domain, with its side chain in close contact with the imidazole ring of the catalytic His 275 (Fig. 3). In the crystal structure, a water molecule bridges the interaction between O $\delta$ 2 of Asp 131 and N $\delta$ 1 of His 275. Asp 131 could, however, easily take over the function of Asp 246 by a simple rotation around its  $\chi$ 1 and  $\chi$ 2 side chain torsion angles, which would allow its side chain to be directly hydrogen-bonded to His 275 N $\delta$ 1. This suggestion is strongly supported by the observation that a similar shift in the topological position of the acidic member of the catalytic triad from the loop after strand  $\beta$ 7 to the loop after strand  $\beta$ 6 is not unusual within the  $\alpha/\beta$  hydrolase fold family [15].

The availability of the first epoxide hydrolase three-dimensional structure suggested new mutation experiments on residues located in the active site, which could not easily be identified from sequence alignments only. For instance, site-directed mutations were performed on Tyr 152 and Tyr 215 to

verify their involvement in catalysis. Only a double Tyr → Phe mutant appeared to be completely inactive, suggesting that both Tyr 152 and Tyr 215 are able to provide the proton needed for the opening of the epoxide ring. Furthermore, a Tyr 215 → Phe mutant displayed a surprising increase in enantioselectivity with styrene oxide (SO), and substituted variants thereof [19]. The  $E$ -value of the mutant enzyme for SO, *m*-chlorostyrene oxide, and *p*-nitrostyrene oxide were increased approximately twofold compared to the  $E$ -value of wild-type enzyme, whereas for *p*-chlorostyrene oxide (*p*ClISO), a spectacular fourfold improvement was observed. The  $k_{\text{cat}}$  values with the (*R*)-enantiomers were hardly affected, and the Tyr 215 → Phe mutant enzyme remained an excellent catalyst, considering that a low concentration of this mutant (3 μM) is still sufficient to convert (*R*)-*p*ClISO (5 mM) in a reasonable amount of time (20–40 min). A possible explanation for this increased enantioselectivity of the mutant can be found in the large increase of  $K_{\text{m}}$  for (*R/S*)-SO, whereas the  $k_{\text{cat}}$  is only slightly reduced for (*R*)-SO, but much more for (*S*)-SO. Therefore, the absence of the Tyr 215 hydroxyl group strongly reduces the stabilization of the transition state and/or the Michaelis complex, leading to lower alkylation rates. In the case of the (*S*)-enantiomer, which is already the poorer substrate for the wild-type enzyme [12], the alkylation rate of the Tyr 215 → Phe enzyme has become rate-limiting, and the resulting relatively strong reduction of the  $k_{\text{cat}}/K_{\text{m}}$  for the (*S*)-enantiomer enhances the enantioselectivity [19].

#### 4. Conclusions

The X-ray structure of Ephy has revealed for the first time the fold of an epoxide hydrolase, and it provides novel, detailed information on the residues involved in the enzymatic mechanism. It located the catalytic residues, the hydrolytic water molecule, the position of the oxyanion hole, and it proposed a possible backup for the acidic member of the catalytic triad. Most importantly, it unambiguously identifies the previously unanticipated Tyr 152/Tyr 215 as the acidic group responsible for binding and possibly protonation of the transition state towards

the formation of the ester intermediate. Furthermore, mutation of Tyr 215 enhanced the enzyme's enantioselectivity towards styrene oxide and substituted variants thereof, making epoxide hydrolase from *A. radiobacter* AD1 potentially interesting for kinetic resolution applications [21].

Since the residues important for catalysis are conserved within the epoxide hydrolase family, it is likely that the structural features found for Ephy are shared by other epoxide hydrolases and therefore allow us to gain a general better understanding of the behaviour and mechanism of this class of biologically and biotechnologically important enzymes.

#### Acknowledgements

Financial support was obtained from the European Union (EU lipase contract no. BI02-CT94-3013). We thank A. Savoia and the staff of the X-ray diffraction beamline at the ELETTRA synchrotron, Trieste (I), for the synchrotron data collection facilities and assistance. Work at the ELETTRA synchrotron was supported by the European Union, contract no. ERBFMGECT950022.

#### References

- [1] A. Archelas, R. Furstoss, *Top. Curr. Chem.* 200 (1999) 159–192.
- [2] G.M. Lacourciere, R.N. Armstrong, *J. Am. Chem. Soc.* 115 (1993) 10466–10467.
- [3] B.D. Hammock, F. Pinot, J.K. Beetham, D.F. Grant, M.E. Arand, F. Oesch, *Biochem. Biophys. Res. Commun.* 198 (1994) 850–856.
- [4] R. Rink, M. Fennema, M. Smids, U. Dehmel, D.B. Janssen, *J. Biol. Chem.* 272 (1997) 14650–14657.
- [5] M. Arand, D.F. Grant, J.K. Beetham, T. Friedberg, F. Oesch, B.D. Hammock, *FEBS Lett.* 338 (1994) 251–256.
- [6] M. Arand, H. Wagner, F. Oesch, *J. Biol. Chem.* 271 (1996) 4223–4229.
- [7] L.T. Laughlin, H.-F. Tzeng, S. Lin, R.N. Armstrong, *Biochemistry* 37 (1998) 2897–2904.
- [8] H.-F. Tzeng, L.T. Laughlin, R.N. Armstrong, *Biochemistry* 37 (1998) 2905–2911.
- [9] M. Arand, F. Müller, A. Mecky, W. Hinz, P. Urban, D. Pompon, R. Kellner, F. Oesch, *Biochem. J.* 337 (1999) 37–43.
- [10] J.H. Lutje Spelberg, R. Rink, R.M. Kellogg, D.B. Janssen, *Tetrahedron: Asymmetry* 9 (1998) 459–466.

- [11] E. Misawa, C.K.C. Chan Kwo Chion, I.V. Archer, M.P. Woodland, N.Y. Zhou, S.F. Carter, D.A. Widdowson, D.J. Leak, *Eur. J. Biochem.* 253 (1998) 173–183.
- [12] R. Rink, D.B. Janssen, *Biochemistry* 37 (1998) 18119–18127.
- [13] R.J. Kazlauskas, H.K. Weber, *Curr. Opin. Chem. Biol.* 2 (1998) 121–126.
- [14] M. Nardini, I.S. Ridder, H.J. Rozeboom, K.H. Kalk, R. Rink, D.B. Janssen, B.W. Dijkstra, *J. Biol. Chem.* 274 (1999) 14579–14586.
- [15] M. Nardini, B.W. Dijkstra, *Curr. Opin. Struct. Biol.* 9 (1999) 732–737.
- [16] D.L. Ollis, E. Cheah, M. Cygler, B. Dijkstra, F. Frolow, S.M. Franken, M. Harel, S.J. Remington, I. Silman, J. Schrag, J.L. Sussman, K.H.G. Verschueren, A. Goldman, *Protein Eng.* 5 (1992) 197–211.
- [17] R. Rink, J. Kingma, J.H. Lutje Spelberg, D.B. Janssen, *Biochemistry* (1999) (in press).
- [18] P.J. Goodford, *J. Med. Chem.* 28 (1985) 849–857.
- [19] R. Rink, J.H. Lutje Spelberg, R.J. Pieters, J. Kingma, M. Nardini, R.M. Kellogg, B.W. Dijkstra, D.B. Janssen, *J. Am. Chem. Soc.* 121 (1999) 7417–7418.
- [20] M.A. Argiriadi, C. Morisseau, B.D. Hammock, D.W. Christianson, *Proc. Natl. Acad. Sci. U. S. A.* 96 (1999) 10637–10642.
- [21] R. Rink, J.H. Lutje Spelberg, R.J. Pieters, J. Kingma, M. Nardini, R.M. Kellogg, B.W. Dijkstra, D.B. Janssen, *European Patent No. 98204315.0* (1999).
- [22] P. Kraulis, *J. Appl. Cryst.* 24 (1991) 946–950.